The Canadian Mineralogist
Vol. 31, pp. 637-647 (1993)

CHEMICAL CHARACTERIZATION OF OSCILLATORY ZONING AND OVERGROWTHS IN ZIRCON USING 3 MeV μ-PIXE

NORMAN M. HALDEN AND FRANK C. HAWTHORNE

Department of Geological Sciences, University of Manitoba, Winnipeg, Manitoba R3T 2N2

JOHN L. CAMPBELL, WILLIAM J. TEESDALE, JOHN A. MAXWELL AND DEREK HIGUCHI

Department of Physics, University of Guelph, Guelph, Ontario N1G 2W1

ABSTRACT

We have used 3 MeV μ-PIXE to chemically characterize mm-scale oscillatory zoning and overgrowths in large crystals of zircon from the Silinjarvi carbonatite, Finland, and a granitic pegmatite from Brazil. The zircon crystals are optically continuous in plane-, cross-polarized and reflected light; oscillatory zoning and overgrowths are distinguished using cathodoluminescence microscopy. Purple-, green- and yellow-luminescent oscillatory zones are usually sharply defined and vary from about 1 to 400 μm in width; rare gradational zoning also is observed. In one crystal, external overgrowths cross-cut earlier oscillatory zones and show embayed contacts with earlier growths. New overgrowths also show oscillatory zoning. Analysis of the oscillatory zones and overgrowths by μ-PIXE (3 MeV proton beam 5 μm in diameter) shows the green- and yellow-luminescent zones in the Finnish samples to have similar Zr/Hf ratios of 49 – 54, whereas the Zr/Hf ratio of new overgrowths range from 43 to 46. The yellow-luminescent zones have lower Sc contents (~53–65 ppm) than the green zones (~98–154 ppm). Overgrowths have low Sc contents (21 – 49 ppm). In the Brazilian sample, the purple-luminescent core has the highest rare-element content (where Y, Th, U, Gd, Dy, Er and Yb are about 2500, 1500, 1000, 130, 300, 340 and 480 ppm, respectively); this grades to a zoned region with yellow-luminescent bands where the Y, U and Th levels are generally lower (1900–2300, 360–900 and 400–700 ppm, respectively). In the outermost zoned overgrowth, Y and Yb contents are about 300 and 80 ppm, respectively, with all other rare elements being below their limits of detection.

Keywords: μ-PIXE, zircon, oscillatory zoning, trace elements, cathodoluminescence, coupled substitutions.

SOMMAIRE

Nous avons utilisé l'émission de rayons X induite par faisceau de protons à 3 MeV (μ-PIXE) pour caractériser chimiquement la zonation oscillatoire et les surcroissances de gros cristaux de zircon provenant de la carbonatite de Silinjarvi, en Finlande, et d'une pegmatite granitique brésilienne. Les cristaux de zircon font preuve de continuité optique en lumière polarisée ou réfléchie; la zonation oscillatoire et les surcroissances deviennent apparentes en cathodoluminescence. Des zones oscillatoires à luminescence violette, verte et jaune sont généralement nettement définies et varient de 1 à 400 μm en largeur. Les gradations en composition s'avèrent plus rares. Dans un cristal, les surcroissances externes recoupent des zones oscillatoires antérieures, comme le révèlent les contacts "en caries". Les surcroissances aussi montrent une zonation oscillatoire. Les analyses avec un faisceau de protons de 5 μm montrent que les zones à luminescence verte et jaune des échantillons finlandais ont un rapport Zr/Hf semblable, entre 49 et 54, tandis que pour les surcroissances, il varie entre 43 et 46. Les zones à luminescence jaune ont une teneur en Sc plus faible (~53 – 65 ppm) que celles qui sont vertes (~98 – 154 ppm). Par contre, les surcroissances possèdent une teneur encore plus faible (21 – 49 ppm). Dans l'échantillon brésilien, le coeur à luminescence violette montre les teneurs les plus élevées en éléments rares (en ppm, Y 2500, Th 1500, U 1000, Gd 130, Dy 300, Er 340, et Yb 480). Vers la bordure, il y a ensuite transition à une séquence de zones de bandes à luminescence jaune; les teneurs en Y, U et Th y sont généralement plus faibles (1900 – 2300, 360 – 900 et 400 – 700 ppm, respectivement). Dans la surcroissance, qui montre aussi une zonation, les teneurs en Y et Yb sont environ 300 et 80 ppm, respectivement, et la teneur de tous les autres éléments rares est inférieure à leur seuil de détection.

(Traduit par la Rédaction)

Mots-clés: zircon, zonation oscillatoire, analyse par μ-PIXE, éléments traces, cathodoluminescence, substitution couplée.

INTRODUCTION

Zircon is an important accessory mineral in many crustal rocks. It occurs as a primary mineral in igneous rocks, and as detrital and recrystallized grains in sedimentary and metamorphic rocks. Many zircon crystals show evidence of intricate growth-histories in the form of complex patterns of zoning and overgrowths

(Vavra 1990, Bowring *et al.* 1989). Such textures can include many different generations of overgrowths, patterns of oscillatory zoning, epitactic outgrowths and crystal forms. These patterns are a record of the physical and chemical conditions prevalent during crystallization of the mineral. The problems in distinguishing the physical and chemical characteristics of such overgrowths and zones are twofold: (1) zonation is commonly on a scale of μm, making a microprobe technique mandatory for its characterization; (2) it can arise from the incorporation of trace elements into the mineral's structure, thus requiring an analytical technique suited to trace elements. The combination of these two requirements can negate the use of routine methods of analysis such as *E*lectron-*P*robe *M*icro*A*nalysis (EPMA), *I*nstrumental *N*eutron *A*ctivation *A*nalysis (INAA) and *I*nductively *C*oupled *P*lasma *M*ass *S*pectrometry (ICP–MS) unless the latter makes use of laser ablation (Jackson *et al.* 1992).

Zircon can incorporate a wide range of trace elements of appropriate valence and atomic radius, including the rare-earth elements (*REE*), U and Th. It is one of the few minerals that has high partition-coefficients for the heavy *REE*, and so its crystallization can affect the chemical evolution of a magma with regard to these elements. The incorporation of U and Th in zircon is important in two ways. Firstly, zircon is used extensively for U–Pb geochronology (Krogh 1982, Bowring *et al.* 1989) owing to its relatively high content of U. Secondly, the localized damage due to alpha particles associated with radioactive decay of the incorporated radionuclides makes the resulting structure more susceptible to secondary alteration (Chakoumakos *et al.* 1987). The geochronological and petrological importance of U, Th and *REE* incorporation in zircon has tended to obscure the fact that these elements compete for their sites in zircon against a wide range of other elements. Speer (1980) discussed the extensive range of trace-element substitutions, involving the alkalis and alkaline earths, transition metals, Be, B, S, Ga, As, Sn, Sb, W, Ag, Au, Sc and Y, many of which could be involved in complex coupled substitutions involving other trace elements (*e.g.*, P and Al). The full range of possible substitutions is not well characterized, a problem made even more difficult by the complex patterns of zoning and overgrowth common in zircon.

EPMA provides a sufficiently small scale of analysis, but insufficient sensitivity for trace elements. Some ablation techniques provide good sensitivity for trace-element microanalysis (*e.g.*, Reed 1990), but are destructive (in that they ablate a pit ~10–30 μm wide depending on the material being analyzed). *P*roton-*I*nduced *X*-ray *E*mission conducted with a focussed microbeam (μ-PIXE) is capable of nondestructive analysis for trace elements, with a beam spot of 5 μm over a wider range of elements than EPMA. The μ-PIXE technique has been used for the analysis of sulfide minerals (Cabri 1988, Cabri *et al.* 1985), phosphate minerals (Rogers *et al.* 1984, Roeder *et al.* 1987, Durocher *et al.* 1988), and silicate minerals (*e.g.*, Griffin *et al.* 1988, Green *et al.* 1989, O'Reilly *et al.* 1991). Here we use μ-PIXE to determine trace-element variations in zircon; the spatial resolution and sensitivity of this technique are sufficient to distinguish between small-scale oscillatory zones and overgrowths.

Sample Description and Preparation

Three crystals of zircon were used in this study: The first, taken from the Mineralogy Museum at the University of Manitoba, and referred to as BZ, is from a collection of zircon crystals from Brazilian granitic pegmatites; it is similar in appearance to zircon crystals from the Novo Horizonte region, but the particular location is unknown. It is euhedral and 2 cm along the *c* axis, reddish and fractured, with alteration along the fractures; between the fractures, the zircon is fresh. The crystal was cut parallel to its *c* axis. It is optically continuous in plane- and cross-polarized and reflected light. Faint zoning is discernable parallel to crystal faces. These zones were distinguished by small narrow fractures that extend the width of the zones, and that are oriented orthogonal to the zones (*cf.* Chakoumakos *et al.* 1987).

The other crystals are from the Silinjarvi carbonatite complex, 20 km north of Kuopio, eastern Finland (Puustinen 1971). The complex, which is mined for apatite as fertilizer, is a tabular body of glimmerite, syenite and sövite; it intrudes Archean granite gneiss. A syenite intrusion that is marginal to sovitic carbonatite is surrounded by phlogopite + alkali-amphibole glimmerite. Zircon is commonly found as an accessory phase in the glimmerite. Two crystals (subsequently referred to as Z1 and Z2) were prepared for analysis. They are subhedral, pale brown, fractured and 2 – 3 cm across. They are macroscopically homogeneous and free of major inclusions, although a number of small μm-scale fluid inclusions were seen. They are optically continuous in reflected, plane- and cross-polarized light (Fig. 1).

Sample preparation

Samples were prepared as doubly polished thin sections ~50 μm thick. They were mounted on glass slides using piccolyte® and then carbon-coated to prevent charge build-up during analysis.

Bulk samples of the Finnish crystals were analyzed by INAA, direct coupled plasma (DCP) and X-ray fluorescence (XRF). Although care was taken to hand-pick the most homogeneous fragments of crushed zircon, it is impossible to discount the possibility of contamination from the incorporation of inclusions.

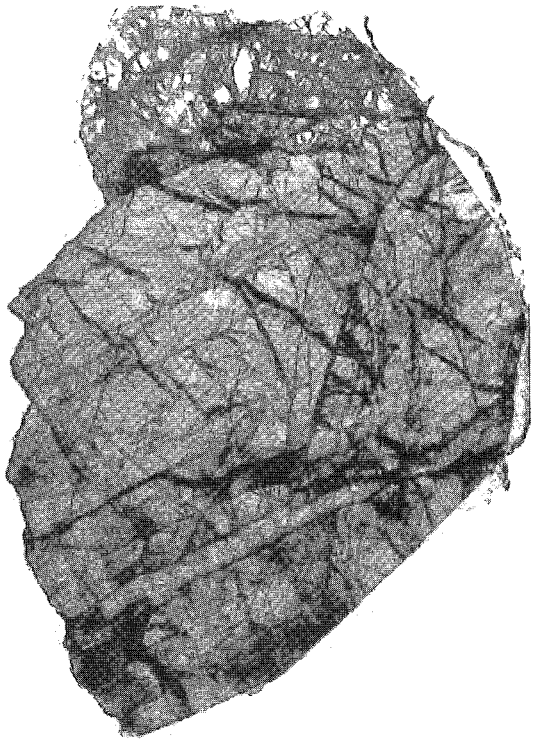

FIG. 1. Photograph of sample Z2 (plane-polarized light); it is optically homogeneous, with fracturing being the only obvious internal structure. The crystal measures 23 × 19 mm.

ANALYTICAL METHODS

μ-PIXE

This work was done at the University of Guelph Van de Graaff accelerator facility. A 5 × 5 μm 3 MeV proton beam was used, with an average beam-current of approximately 0.5 nA; the resulting X-ray spectra were recorded with a Si(Li) detector. The time-integrated charge for each analysis was 2 μC. A 0.125-mm mylar filter was used to suppress low-energy background radiation together with the intense zirconium *L* and silicon *K* X-rays. A tantalum collimator limited the detector's field of view in order to exclude X rays scattered from materials in the specimen chamber. Spectra were processed using the Guelph PIXE software package GUPIX (Maxwell *et al.* 1989). Elemental concentrations are derived from the intensities of various X-ray peaks through established mathematical and physical relationships involving X-ray generation and associated matrix effects (including secondary fluorescence); this approach (Campbell *et al.* 1990) resembles the better-known methodology of electron-probe microanalysis. The overall standardization of the system was done using Zr and Ta metal standards and a well-characterized synthetic pyrrhotite standard (provided by CANMET) containing 0.1% each of Se and Pd.

GUPIX extracts peak areas from the spectrum by a nonlinear least-squares-fitting procedure (Maxwell *et al.* 1989). A model spectrum is constructed using estimated concentrations and a database that includes relative X-ray intensities for each element. The continuum background is removed from the measured spectrum by the top-hat filter method. Concentrations of all elements observed in the spectrum are iterated until the best fit between measured and model spectra is attained. The X rays of oxygen and silicon are not observed, but these elements play a role in the proton–specimen and photon–specimen interactions; the concentration of the SiO_4 complex is therefore taken as 100% less the summed concentrations of all observed elements. Concentrations are iterated until the best fit between model and measured spectra is attained.

In the model spectrum, the peaks are represented by Gaussians with exponential low-energy-tailing features. However, the intense *K* X-ray peaks of zirconium exhibit an additional shelf-like low-energy feature that arises from Compton scattering of X rays whose original direction was other than toward the detector; the low-energy cutoff of this feature corresponds closely to the energy loss incurred in 180° Compton scatter. In order to obtain reliable results for yttrium, whose *K* X-ray is superimposed on this feature, a second set of fits was performed. These were restricted to the X-ray energy region 12 – 19.5 keV, and the shelf feature was modeled on the basis of measurements on pure zirconium metal. Examples of fits are given below, but we note here that because of the shelf, the limit of detection for yttrium is about 100 ppm.

The proton-induced X-rays are augmented by secondary X-rays arising from fluorescence of trace elements by the intense *K* X-rays of Zr. In a homogeneous matrix of zircon of infinite extent, the fractional enhancement is 9.6% for Y, 7% for U, 5% for Th, 1.6% for Hf, and considerably less in all other cases. Since the attenuation length of the Zr *K* X-rays in zircon is about 160 μm, there is the possibility that the fluorescence contributions will differ from these values owing to contributions from neighboring zones of differing trace-element content. To minimize the possibility of exciting adjacent zones, only zones in excess of 50 μm across were analyzed. The variations in concentration of interest (see below) were significantly larger than the potential errors attributed to secondary fluorescence indicated above.

Cathodoluminescence microscopy

The cathodoluminescence (CL) images were


2a

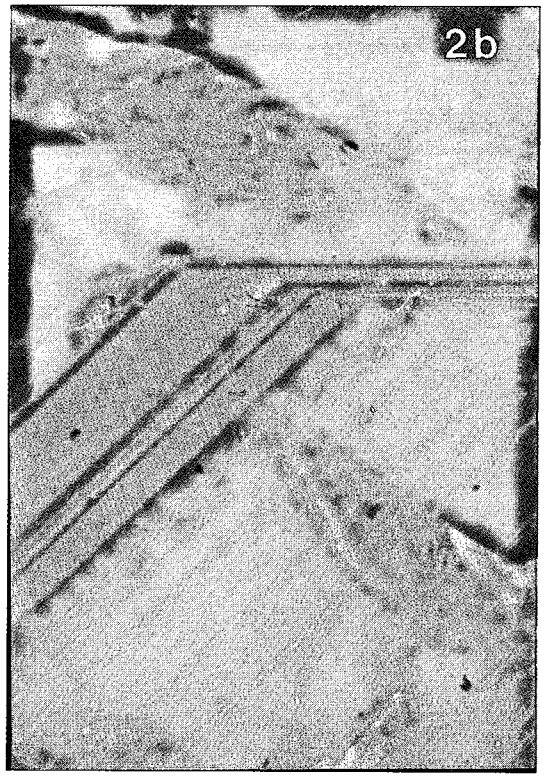
2b

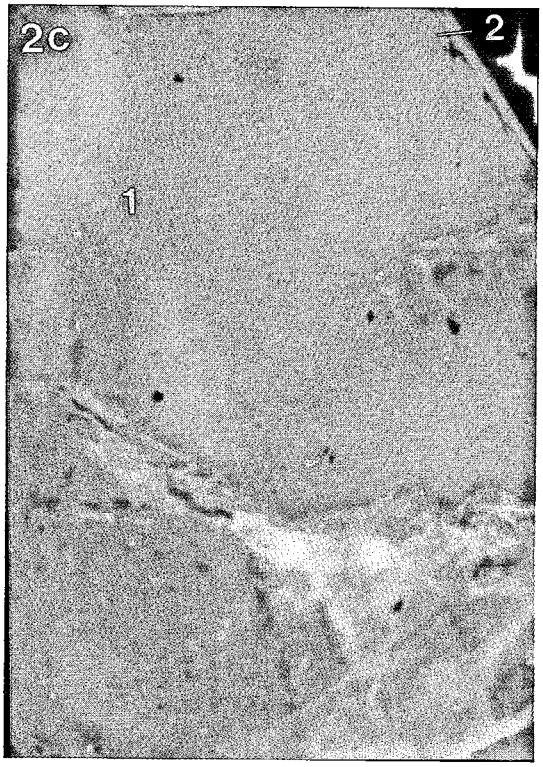
2c
2
1


2d

recorded using a TECHNOSYN cold-cathode luminescent unit operating at 20 kV, with an average gun current of 400 μA. The CL and photomicrograph work was done on the polished sections prior to the application of the carbon coating.

RESULTS

Cathodoluminescence microscopy

Although the zircon crystals are relatively homogeneous in transmitted and reflected light, cathodoluminescence microscopy showed the presence of extensive oscillatory zoning and overgrowths. The zircon from Brazil can be divided into two regions characterized by luminescence and zoning: (i) a homogeneous internal region of purple luminescence that grades to a region with yellow-luminescent oscillatory zoning at its outer margin; (ii) a mantle dominated by yellow- to grey-luminescent oscillatory zoning alternating in intensity (Fig. 2a). In the internal region, the change from the dominantly purple to dominantly yellow luminescence is symmetrical about the contact between the regions. At the outer margin of the purple region, yellow oscillations first appear and increase until they eventually dominate, and the purple zones gradually disappear.

Oscillatory zones vary in thickness from about 10 to 100 μm, and boundaries may be sharp or diffuse. The zones distinguished by the orthogonal fractures show bright yellow-luminescent lines that cut through the center of the fractures; on either side of the bright line, there is a diffuse region of yellowish luminescence.

The zircon crystals from Finland show no internal structure in plane-polarized light except for extensive fracturing (Fig. 1). Figure 2b shows green- and yellow-luminescent zones whose orientation corresponds to that of crystal faces. The thickness of the zones can vary between ~1 and 400 μm; contacts between zones are usually sharp. Figure 2c shows two overgrowths in sample Z2. The first overgrowth shows a pronounced lobe attributed to resorption that cuts into the earlier-formed part of the crystal; oscillatory zones cut by this lobe are continuous on either side of the lobe. The outermost region of new growth is a thin, structureless region that luminesces pale green; it cross-cuts oscillatory zoning in the first overgrowth.

Both crystals (Z1 and Z2) show pervasive oscillatory zoning; in sample Z1, some particularly distinctive zones can be traced around the whole crystal. Figure 2d shows part of an unusually wide zone (approximately 400 μm). At the bottom of this view, there is a relatively abrupt change from a region that luminesces dominantly green with some minor yellow-luminescent zoning to an almost featureless yellow-luminescent region, the upper boundary of which is characterized by the onset of fairly uniform oscillatory zoning. These boundary features can be traced around the whole crystal. Some preliminary spectroscopic measurements carried out within the yellow region showed a broad band of intrinsic cathodoluminescence that centered at a wavelength of ~560 nm. There were no obvious peaks that could be associated with activator elements.

Bulk geochemical analysis of the zircon from Finland

Results of bulk analyses of zircon Z1 and the host glimmerite are shown in Table 1. Concentrations of U,

TABLE 1. BULK CHEMICAL COMPOSITION OF ZIRCON Z1 AND GLIMMERITE HOST-ROCK GC-1

		Z1	GC-1			Z1	GC-1	
SiO_2	wt%	32.08	40.80		La ppm	4	57	(0.10)
Al_2O_3		0.08	5.79		Ce	----	138	(1.00)
TiO_2		0.19	0.14		Nd	----	55	(3.00)
Fe_2O_3		0.15	10.20		Sm	0.6	9.6	(0.01)
MnO		----	0.07		Eu	0.7	2.8	(0.05)
CaO		0.86	6.53		Yb	9.1	0.2	(0.05)
MgO		0.14	19.70		Lu	0.2	----	(0.01)
K_2O		0.06	6.43					
P_2O_5		0.31	3.36		Hf	8300	3.2	(0.20)
ZrO_2		65.60	----		Th	4.3	0.9	(0.20)
LOI		1.08	4.23		U	10.3	----	(0.10)
					Y	1420	----	(10.0)
Sc	ppm	64	32	(0.01)	Nb	536	42	(10.0)
V		56	64	(2.00)	Zr	----	536	(10.0)
Mn		32	--	(2.00)				
Co		--	27	(0.50)				
Cu		5	3	(0.50)				
Zn		4	68	(0.50)				
Rb		--	240	(10.0)				
Sr		900	900	(100)				
Ba		434	55	(10.0)				

Limits of detection of trace and minor elements are given in parentheses. The concentration of Sc, Rb, Sr, the rare earths, Hf, Th and U was determined by INAA. The concentration of V, Mn, Co, Cu and Zn was determined by DCP. The concentration of all other elements was determined by XRF.

FIG. 2 (a) Pale yellow and purple cathodoluminescence and oscillatory zoning in sample BZ. The internal region is dominated by purple luminescence, but it also shows thin bands of yellow luminescence fringed by diffuse yellow luminescence. These bands correspond to the distribution of fractures; the fractures span the width of the diffuse yellow luminescence and are oriented at 90° to the luminescent bands. The marginal region shows fine-scale (5–20 μm) yellow oscillatory zoning. The white scale-bar in the upper right of the picture is 100 μm; Figures 2b, c and d are at the same scale. (b) Sample Z2 showing typical yellow and green cathodoluminescence and oscillatory zoning. (c) Overgrowths in sample Z2, labeled "1" and "2". Overgrowth 1 shows a pronounced resorption-related lobe in contact with the earlier-formed part of the crystal. Overgrowth 2 is a thin region at the margin of the crystal that cross-cuts oscillatory zoning in overgrowth 1. (d) A wide (~400 μm), virtually featureless zone in sample Z1; the internal contact of this zone is relatively sharp, the outside contact is characterized by the gradational onset of oscillatory zoning. The zone is continuous and can be traced around the whole crystal.

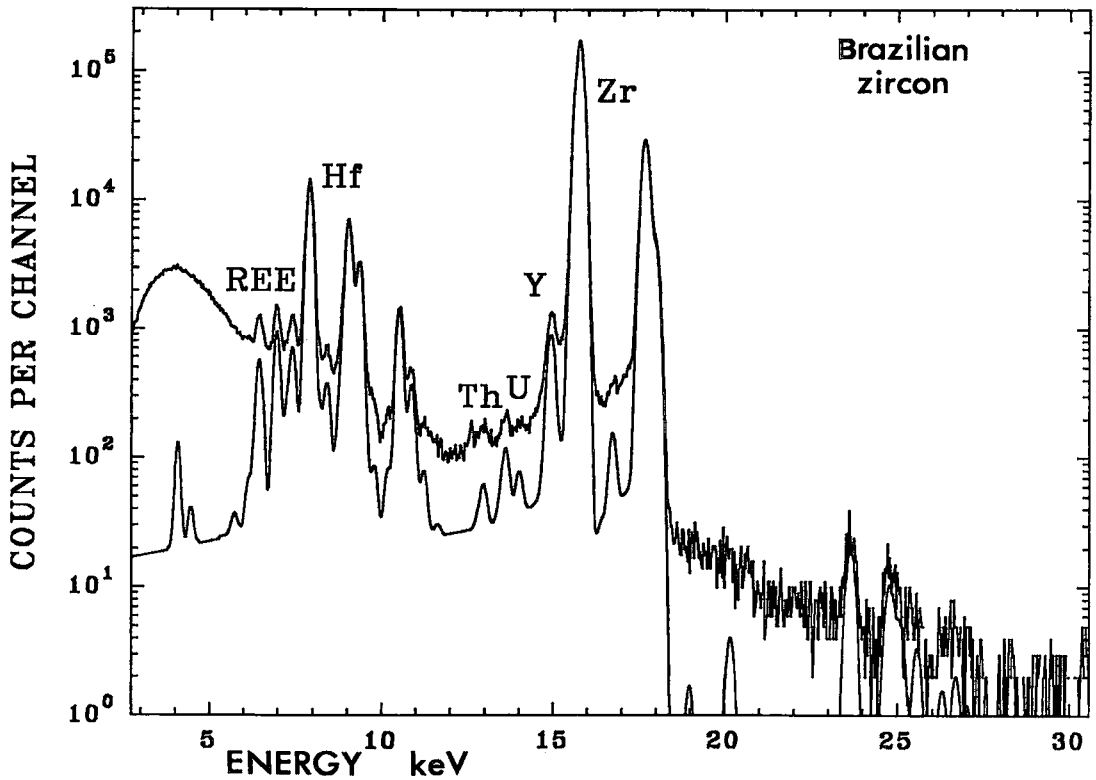

FIG. 3. μ-PIXE spectrum collected from the Brazilian zircon; it shows the Zr*K*α and *K*β X-rays and Hf*L* X-rays. The Y*K*α X-ray is a distinct peak on the side of the Zr*K*α X-ray peak, and the Y*K*β X-ray line is clearly visible. The *L* X-rays of U and Th can be seen between the Zr and Hf X-rays, and the *L*αX-rays of Dy, Er and Yb (labeled *REE*) can be seen on the low-energy side of the Hf X-ray lines.

Pb and the *REE* are very low, and there is relative enrichment of the heavy *REE* consistent with known partition coefficients for the *REE*. The Sc content (64 ppm) is similar to that obtained in the PIXE analysis (see below), but the Y content of 1410 ppm was not seen in the PIXE analyses, and so may indicate contamination by inclusions (possibly xenotime). The levels of U, Pb and the *REE* are all below the detection limits for μ-PIXE (*cf.* Campbell *et al.* 1990).

μ-PIXE

Figure 3 shows an X-ray spectrum from the purple-luminescent central region of the crystal from the Brazilian granitic pegmatite. The Y*K*α X-ray is visible on the low-energy side of the Zr*K*α X-ray peak (at a position that would correspond to the Compton scattering shelf described earlier), and the Y*K*β line can be seen between the Zr X-ray lines. In addition, the *L* X-rays of U, Th, Gd, Dy, Er and Yb also are visible. Figure 4 shows the peak fit, residuals and data fit over the 14 – 19 keV region (after careful measurement of the Zr X-ray line shapes and accounting for the shape of the low-energy Compton shelf feature); this improves the fit of the spectrum in this region.

Figure 5 shows a *S*canning *P*roton *M*icroprobe (SPM) line-scan that was used to help locate the beam for point analyses 7, 8 and 9 (Table 2). The scan was perpendicular to a yellow-luminescent zone and parallel to one of the orthogonal fractures. The scan shows: (i) an increase in Zr and Hf, in this case, toward the outside of the crystal, with an apparently constant Zr/Hf ratio (Figs. 5a, b), (ii) low Σ*REE* values in the center of the scan, with slightly higher, and variable levels at the ends (Fig. 5c), and (iii) decreasing U + Th toward the outside of the crystal (Fig. 5d); if the U and Th scans are separated, there is a slight U peak in the center of the scan. The center of the scan should correspond to the location of a bright yellow-luminescent line.

Table 2 shows the resulting analytical data from the μ-PIXE spectra taken from the core, the zoned region with the fractures and the overgrowth showing oscillatory zoning. The 1σ errors represent the precision of the fitting procedure in determining peak intensities; the error incurred in standardization involves contri-

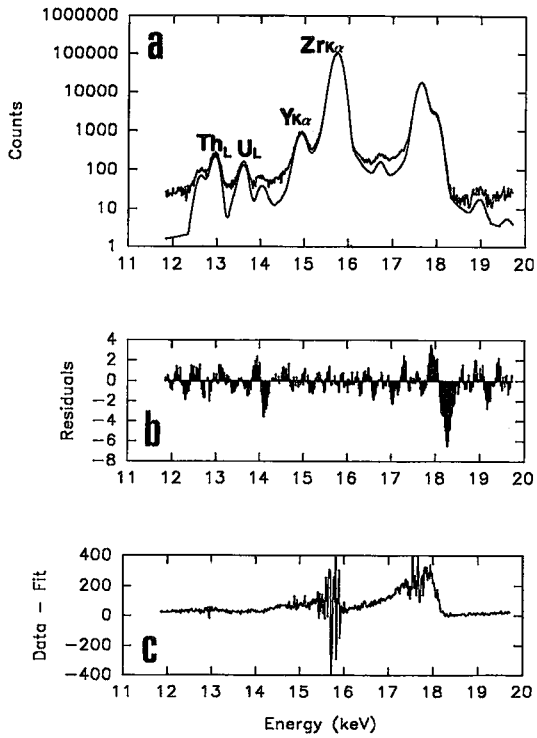

FIG. 4. Expansion of the 11 – 20 keV region of one of the spectra to show the effect of fitting the Zr *K* X-rays with line shapes determined from pure Zr.

butions from the database and the detector properties, and is estimated at about 2% for Zr and Hf, and 5% for trace elements. The Zr/Hf ratio is reproducible to within 0.5%.

The core region has the highest rare-element content (except for one analysis in the zoned region) and the outer overgrowth, the lowest rare-element content. The sites of analyses 1, 2 and 3 were located optically (in reflected light) with respect to an orthogonal fracture; analysis 2 was carried out in the center and was assumed to correspond to the location of a yellow-luminescent zone. It was not possible to check the exact location as reference to a pattern of luminescence was not possible with the narrow proton beam. There is a general decrease in rare elements toward the outside of the crystal. Analyses 7, 8 and 9 were carried out on a different zone. These points were located using SPM as a guide (Fig. 5c); again, there is a general decrease in the rare elements toward the outside of the crystal.

Although Figure 5 shows significant variability in concentration of the *REE*, U and Th of a zone over a scan of 100 μm (and in the case of the *REE* variability, on a scale comparable with the changes in luminescence), further work would be required to check the exact correspondence of luminescence and elemental abundance.

Figure 6 shows a typical μ-PIXE spectrum (over the 3 – 12 keV region) collected from one of the darker green-luminescent bands in sample Z2 from Finland. The principal X-ray lines observed are the *L* X-rays of Hf. The small peak corresponds to the *K*α X-ray of Sc. The spectrum was found to be simpler than that of the Brazilian zircon, no other trace elements being present.

Tables 3 and 4 show the quantitative measurements resulting from the μ-PIXE spectra. Each table includes an average concentration of a zone based upon four closely spaced analytical points to provide an estimate of analytical variation for each element. For samples Z1 and Z2, there is little variation in Zr/Hf ratio between the yellow- and green-luminescent areas. In sample Z2, there is a change in Zr/Hf ratio corresponding to the regions of new growth (labeled 1 and 2 on Fig. 2c), in which the Zr/Hf ratio falls to as low as 43. It should be noted that quantitative EPMA of these regions showed no systematic variation in the Zr/Hf ratio. The yellow-luminescent zones have lower contents of Sc (53 – 65 ppm) than the green-luminescent areas (in which the Sc contents can be as high as 98 – 154 ppm). The most significant variation in trace-element chemistry corresponds to the new growths, in which the Sc concentrations drop to as low as 21 ppm. The variation in the Sc contents between the yellow and green bands is systematic and significant in terms of the analytical variation.

DISCUSSION

In this study, oscillatory zones and overgrowths were observed using cathodoluminescence microscopy and chemically characterized using μ-PIXE in otherwise optically featureless crystals of zircon. The characteristic luminescent colors of the oscillatory zones correlate with differences in Sc content in the zircon crystals from Finland. The green-luminescent areas have higher Sc contents (98 – 154 ppm) than the yellow-luminescent areas (53 – 65 ppm). In the Brazilian zircon, the highest concentrations of trace elements are found in the core region of the crystal. The zones with orthogonal fractures show decreasing trace-element abundances toward the outside of the crystal, with low Σ*REE* levels in the middle of the zones. The correspondence of low U and Th contents in zones with orthogonal cracks is similar to what was observed by Chakoumakos *et al.* (1987). There is no significant variation in the ratio of Zr to Hf in the oscillatory zones of any of the samples. This contrasts with the overgrowth features; in both the BZ and Z2 crystals, the overgrowths cross-cut earlier textural features and have significantly lower Zr/Hf ratios.

In the Finnish zircon, Sc was probably incorporated

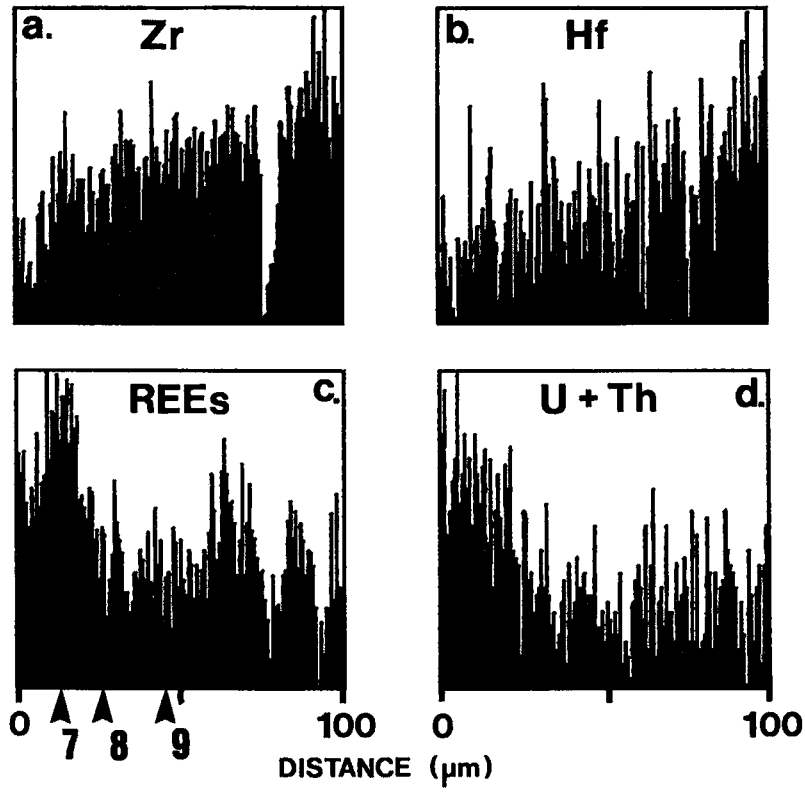

FIG. 5. Scanning Proton Microprobe (SPM) line scan of a zone with orthogonal fractures. The horizontal distance scanned was 100 μm, and the positions of points 7 – 9 analyzed (Table 4) are shown on the bottom of scan c.

into the structure by a coupled substitution involving P: $Sc^{3+} + P^{5+} \rightleftharpoons Zr^{4+} + Si^{4+}$. It was not possible to analyze for P using PIXE because of overlap of Zr *L* X-ray lines on P *K* X-ray lines; in addition, the mylar filter used during analysis suppresses this region of the spectrum. However, P did appear in reconnaissance EPMA analyses of the Finnish zircon. Considering the abundance of P in the host glimmerite, this mechanism of substitution seems likely. In the Brazilian zircon, the range of possible trace-

TABLE 2. μ-PIXE COMPOSITIONS OF ZONES IN BRAZILIAN ZIRCON BZ

	core	1	2	3	7	8	9	og	1σ*	LOD
Zr	54.8	51.1	51.9	51.1	54.5	50.7	51.2	50.6	467	137
Hf	8200	7640	7900	7560	8570	7870	8050	8050	38	138
Zr/Hf	65.8	66.9	65.7	67.7	63.6	64.4	63.7	62.9		
Fe	213	76	48	38	231	130	239	---	4	8
Y	2498	2235	1974	1822	2814	2235	2122	311	37	100
Gd	131	---	---	---	129	---	---	---	12	25
Dy	312	213	182	164	307	224	201	---	17	36
Er	339	286	210	210	338	258	245	---	16	38
Yb	486	487	452	393	497	395	309	84	13	24
ΣREE	1268	986	844	767	1271	877	755	---		
Th	1517	362	362	261	1973	978	723	---	30	46
U	1092	582	419	430	1304	761	714	---	33	52

Zr in wt%; Hf,Fe,Y,Dy,Er,Yb,Th,U in ppm;
Analyses 1 & 3 correspond to purple luminescent zones, analysis 2 to a yellow zone
Analysis points 7 - 9 correspond to the points shown in Figure 5;
LOD : average lower limit of detection in ppm;
--- : below LOD + 3σ.
1σ* : Average error (1σ)in ppm due to spectrum fitting
og : overgrowth

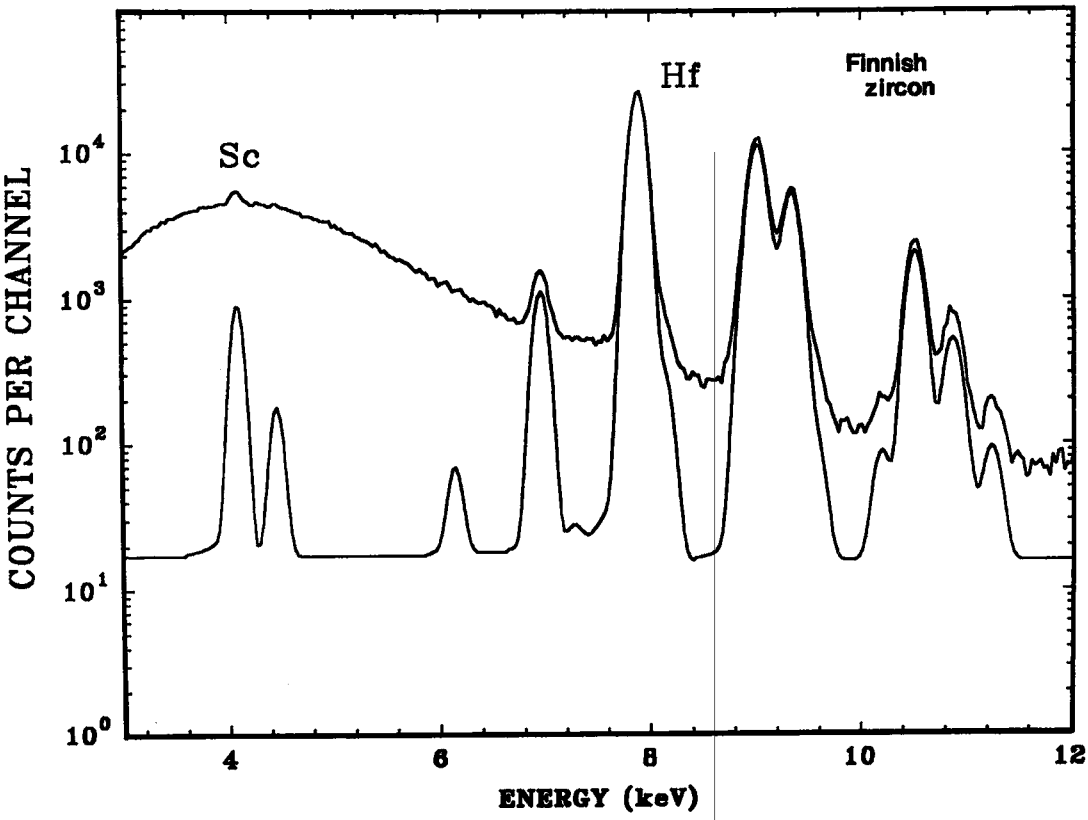

FIG. 6. μ-PIXE spectrum collected from sample Z1, showing Hf *L* X-rays and the Sc*K*αX-ray.

element substitutions is more complicated. In addition to the coupled substitution of $(Y,REE)^{3+} + P^{5+}$ for $Zr^{4+} + Si^{4+}$, there is direct substitution of (U^{4+}, Th^{4+}) for (Zr^{4+}, Hf^{4+}). Both these mechanisms of substitution must have operated at the same time, but, in comparing Figures 5c and 5d, they seem to have produced different patterns.

Oscillatory zoning and overgrowths

The oscillatory zoning in these crystals is extensive and clearly defined. Such zoning has been observed in many other cases (Speer 1980, Bowring *et al.* 1989, Vavra 1990). In the case of the zircon from Finland, the character of the zoning changes from rapid rhythmic oscillations to broad, almost featureless bands to irregular oscillations. The pattern of variation among zones in the Brazilian zircon is symmetrical about the contact between the core and its outer mantle; finally, an overgrowth with small-scale oscillatory zoning has coated the core region.

Using an ion microprobe, Shimizu (1990) determined the chemical characteristics of oscillatory zoning in augite crystals from alkali basalts; variation and oscillations in trace-element chemistry among the zones were found not to be compatible with a simple surface-equilibrium model of crystal growth (Rayleigh fractionation). Some of the ways suggested for generating such zoning include: (1) oscillatory changes in partition coefficients corresponding to temperature fluctuations, (2) repeated injection of new liquids with mixing and new growth, and (3) variations in rate of crystal growth (*cf.* Shimizu 1990).

A similar problem exists with the interpretation of the oscillatory zoning in the zircon crystals in this study. In the case of the crystals from Finland, the overgrowths can be chemically and physically distinguished from oscillatory zoning and can be reasonably interpreted as the result of mixing and reaction with new liquids during growth. The frequency of variations in temperature (and thus in partition coefficient) that would be necessary to produce the thousands of zones observed in Z1, and the extent of variation in temperature that would be necessary to significantly change the partition coefficients, seem physically unreasonable. The effects of changes in the rate of

TABLE 3. μ-PIXE COMPOSITIONS OF ZONES IN ZIRCON Z1

	yellow band	medium band	green band	LOD
Zr	51.0	51.0	50.9	57
Hf	1.03	1.01	1.01	13
Zr/Hf	49.2	50.2	50.2	
Sc	53 ± 7*	76 ± 7	98 ± 7	14

*1σ error due to spectrum fitting
LOD in ppm. LOD's are calculated for each analysis, these are representative values.

Average concentration of a yellow band*

Zr	50.9 ± 0.38	Sc	65 ± 8
Hf	1.02 ± 225		
Zr/Hf	50.0		

Zr in wt %; Hf,Sc in ppm
* based on 4 closely spaced analyses.
Analytical variation shown is 1σ.

crystal growth are difficult to assess because all the elements sought in this study are compatible in zircon; antithetic variations with incompatible elements were not observed.

It is more likely that the oscillatory zones record the effects of a kinetic feedback mechanism (Ortoleva *et al.* 1987) in which the development of the zones has been affected by the differential rate of diffusion of components to the surface of the growing crystal. One of the requirements for such zoning is that at least two processes of diffusion involved in the crystal growth be coupled. In the Finnish crystals, the diffusion and substitution of Sc and P are coupled. In the Brazilian zircon, the diffusion of Y, *REE* and P are coupled and are spatially associated with U and Th substitution. In both cases, variations in trace-element concentrations are repeated on a very small scale, and variations of a similar scale are not observed in the level of major elements present. This suggests that (i) the variation in trace-element concentrations was decoupled from variation in major-element concentrations, and (ii) different mechanisms of substitution may be simultaneously available to the major and trace elements during growth of the crystals.

TABLE 4. μ-PIXE COMPOSITIONS OF ZONES IN ZIRCON Z2

	yellow band		green band	
Zr	51.2	51.1	51.25	51.27
Hf	9610	9620	9500	9430
Zr/Hf	53.3	53.2	54.0	54.4
Sc	65 ± 7*	65 ± 7	121 ± 7	126 ± 7

	New Growth 1		New Growth 2
Zr	50.8	51.18	51.61
Hf	1.09	1.10	1.18
Zr/Hf	46.7	46.2	43.5
Sc	23 ± 7	21 ± 7	49 ± 7

Zr in wt%; Hf,Sc in ppm
* 1σ error due to spectrum fitting, LOD are given in Table 1.

Average concentration of a green band*

Zr	51.1 ± 0.44	Sc	154 ± 7
Hf	1.00 ± 149		
Zr/Hf	53.6		

* based on 4 closely spaced analyses.
Analytical variation shown is 1σ.

CONCLUSIONS

The characterization of oscillatory trace-element zoning in minerals is an important step in understanding diffusion-controlled aspects of the crystallization of minerals. The very fine-scale nature of such textures requires a microprobe technique for their chemical characterization. If the primary components of such zoning are present only at the trace level, stringent constraints are placed on the possible methods of chemical analysis. Routine μ-PIXE currently has a beam diameter of ~5 μm (and ~1 μm is now possible with current modifications in lens designs). The detection limits and the nondestructive nature of the method make it attractive in analysis of materials for trace elements. Here we have shown that the oscillatory zoning observed in the zircon crystals correlates with significant variations in levels of trace elements. This type of oscillatory zoning is presumably connected with nonequilibrium effects associated with differential diffusion of these trace components through the fluid phase to the growing face of the crystal. The μ-PIXE method can provide the basic chemical data necessary for an understanding of this mechanism.

ACKNOWLEDGEMENTS

This work was done with the assistance of a University of Manitoba Research Development Grant and operating grants from the Natural Sciences and Engineering Research Council of Canada to N.M.H., F.C.H. and J.L.C., and an Infrastructure grant to J.L.C. We thank Roger Mason for the cathodoluminescence spectroscopy, and the referees and R.F. Martin for helpful criticism of an earlier version of the manuscript.

REFERENCES

BOWRING, S.A., WILLIAMS, I.S. & COMPSTON, W. (1989): 3.96 Ga. gneisses from the Slave Province, Northwest Territories, Canada. *Geology* **17**, 971-975.

CABRI, L.J. (1988): Applications of proton and nuclear microprobes in ore deposit mineralogy and metallurgy. *Nucl. Instrum. Methods Phys. Res.* **B30**, 459-465.

———, CAMPBELL, J.L., LAFLAMME, J.H.G., LEIGH, R.G., MAXWELL, J.A. & SCOTT, J.D. (1985): Proton-microprobe analysis of trace elements in sulfides from some massive-sulfide deposits. *Can. Mineral.* **23**, 133-148.

CAMPBELL, J.L., MAXWELL, J.A., TEESDALE, W.J., WANG, J.-X. & CABRI, L.J. (1990): Micro-PIXE as a complement to electron probe microanalysis. *Nucl. Instrum. Methods Phys. Res.* **B44**, 347-356.

CHOKOUMAKOS, B.C., MURAKAMI, T., LUMPKIN, G.R. & EWING, R.C. (1987): Alpha-decay-induced fracturing in

zircon: the transition from the crystalline to the metamict state. *Science* **236**, 1556-1559.

DUROCHER, J.J.G., HALDEN, N.M., HAWTHORNE, F.C. & MCKEE, J.S.C. (1988): PIXE and micro-PIXE analysis of minerals at E_p = 40 MeV. *Nucl. Instrum. Methods Phys. Res.* **B30**, 470-473.

GREEN, T.H., SIE, S.H., RYAN, C.G. & COUSENS, D.R. (1989): Proton microprobe-determined partitioning of Nb, Ta, Zr, Sr, and Y between garnet, clinopyroxene and basaltic magma at high pressure and temperature. *Chem. Geol.* **74**, 201-216.

GRIFFIN, W.L., JAQUES, A.L., SIE, S.H., RYAN, C.G., COUSENS, D.R. & SUTER, G.F. (1988): Conditions of diamond growth: a proton microprobe study of inclusions in West Australian diamonds. *Contrib. Mineral. Petrol.* **99**, 143-158.

JACKSON, S.E., LONGERICH, H.P., DUNNING, G.R. & FRYER, B.J. (1992): The application of laser-ablation microprobe – inductively coupled plasma – mass spectrometry (LAM–ICP–MS) to in situ trace-element determinations in minerals. *Can. Mineral.* **30**, 1049-1064.

KROGH, T.E. (1982): Improved accuracy of U–Pb zircon ages by the creation of more concordant systems using the air abrasion technique. *Geochim. Cosmochim. Acta* **46**, 637-649.

MAXWELL, J.L., CAMPBELL, J.L. & TEESDALE, W.J. (1989): The Guelph PIXE software package. *Nucl. Instrum. Methods Phys. Res.* **B43**, 218-230.

O'REILLY, S.Y., GRIFFIN, W.L. & RYAN, C.G. (1991): Residence of trace elements in metasomatized spinel lherzolite xenoliths: a proton-microprobe study. *Contrib. Mineral. Petrol.* **109**, 98-113.

ORTOLEVA, P., MERINO, E., MOORE, C. & CHADAM, J. (1987): Geochemical self-organization. I. Reaction-transport feedbacks and modelling approach. *Am. J. Sci.* **287**, 979-1007.

PUUSTINEN, K. (1971): Geology of the Silinjarvi carbonatite complex, eastern Finland. *Bull. Comm. Géol. Finlande* **249**.

REED, S.J.B. (1990): Recent developments in geochemical microanalysis. *Chem. Geol.* **83**, 1-9.

ROEDER, P.L., MACARTHUR, D., MA, X.-P., PALMER, G.R. & MARIANO, A.N. (1987): Cathodoluminescence and microprobe study of rare-earth elements in apatite. *Am. Mineral.* **72**, 801-811.

ROGERS, P.S.Z., DUFFY, C.J., BENJAMIN, T.M. & MAGGIORE, C.J. (1984): Geochemical applications of nuclear microprobes. *Nucl. Instrum. Methods Phys. Res.* **B3**, 671-676.

SHIMIZU, N. (1990): The oscillatory trace element zoning of augite phenocrysts. *Earth Sci. Rev.* **29**, 27-37.

SPEER, J.A. (1980): Zircon. *In* Orthosilicates (P.H. Ribbe, ed). *Rev. Mineral.* **5**, 67-112.

VAVRA, G. (1990): On the kinematics of zircon growth and its petrogenetic significance: a cathodoluminescence study. *Contrib. Mineral. Petrol.* **106**, 90-99.

Received June 6, 1991, revised manuscript accepted February 8, 1993.